ELSEVIER

Polymer 41 (2000) 1597–1606

polymer

Distribution of individual components in thermoplastic olefins: step-scan FT-IR photoacoustic phase analysis

B.R. Kiland[a], M.W. Urban[a,*], R.A. Ryntz[b]

[a]*Department of Polymers and Coatings, North Dakota State University, Fargo, ND 58105, USA*
[b]*Visteon Automotive Systems, Dearborne, MI 58121, USA*

Received 4 January 1999; accepted 5 May 1999

Abstract

A method to determine surface stratification of components within a thermoplastic olefin (TPO) compound is developed using Fourier transform infrared (FT-IR) step-scan photoacoustic spectroscopy (S^2 PAS). Infrared bands attributed to magnesium silicate (talc), polypropylene (PP), and ethylene–propylene rubber (EPR) are used as analytical depth-profiling probes to establish the origin of the photoacoustic (PA) signal. This was accomplished by performing a series of experiments at various modulation frequencies, and subsequent monitoring of phase spectra and phase rotated spectra generated from signals collected at 0° (*I*) and 90° (*Q*) phase shifted from the light source. Utilizing phase analysis data, a TPO compound stratification model was developed, which consists of four distinct layers extending by 0–12 μm from the sample surface. Layer I (0–3 μm) shows evidence of a large change in talc and PP concentration, while layer II (3–6 μm) shows a significant decrease in both of these components. Within this same layer, evidence of discrete individual EPR particles are shown by an abrupt concentration change from 2.67 to 5.35 μm, followed by a large decrease from 5.35 to 6.55 μm. Further into the sample at 6–9 μm from the surface (layer III), all three components reach their highest maximums for all four layers, with talc serving as the local maximum. Approaching layer IV, talc concentration diminishes until it is no longer apparent further than a distance of 8.40 μm from the surface. In addition, both EPR and PP concentration are detected within this layer (9–12 μm), showing decreases in concentration with depth. The proposed depth profiling technique also shows potential applications to various systems displaying stratification near the surface.

Keywords: Thermoplastic olefins; Step-scan photoacoustic spectroscopy; Fourier transform infrared spectroscopy

1. Theoretical analysis

In photoacoustic (PA) spectroscopy, modulated infrared (IR) light is absorbed by a sample, followed by nonradiative de-excitation processes converting light to heat. Thermal waves produced within a depth *x* travel to the sample surface, periodically heating an adjacent, inert gas atmosphere directly above the surface. A microphone within the gas atmosphere detects pressure fluctuations produced by this periodic heating of the sample, and subsequent Fourier transformation (FT) of the interferogram generates PA FT-IR spectra. An illustration of a PA cell, along with frequently used parameters in a PA system (discussed later), is shown in Fig. 1 [1,2].

Two modes of data collection for PA FT-IR experiments are continuous-scan (CS PAS) and step-scan (S^2 PAS), where the distinction between the two methods depends on whether the modulation frequency is varying, or constant for each wavelength [3]. The expression for the Fourier frequency at a specific wavenumber is defined as [4]:

$$f = 2v\bar{\nu} \tag{1}$$

where *v* is the velocity of the interferometer mirror (cm s^{-1}), and $\bar{\nu}$ is the wavenumber (cm^{-1}). In CS PAS mode, the interferometer mirror moves at a constant velocity for all retardation points, resulting in a different modulation frequency for each wavenumber. Conversely, the mirror moves incrementally to each retardation point in S^2 PAS experiments, where application of a constant light frequency eliminates spectral multiplexing of the instrument often found when using CS PAS [5].

S^2 PAS experiments can be further classified according to the method used to produce a modulated light waveform, which are amplitude modulation (AM) and phase modulation (PM) [6]. In AM experiments, a beam chopper (mechanical interference) produces modulated radiation, whereas PM utilizes oscillation of the interferometer mirror

* Corresponding author. Tel.: +1-701-231-7859; fax: +1-701-231-8439.
E-mail address: urban@plains.nodak.edu (M.W. Urban)

0032-3861/00/$ - see front matter
PII: S0032-3861(99)00323-7

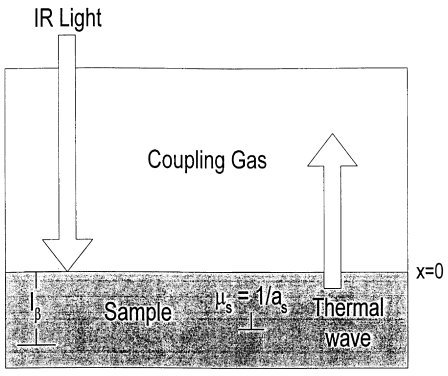

Fig. 1. Schematic diagram of a PA cell, along with optical and thermophysical properties of the system.

back and forth across a set point (light interference) for signal generation. Both methods effectively modulate the IR light source, but PM modulation allows continuous irradiation, resulting in a higher signal-to-noise ratio. Moreover, AM experiments produce a large direct-current (dc) offset, resulting in substantial noise contributions outside the zero-path-difference point of the interferogram (i.e. the "wings" on the sides of the centerburst region), creating significant spectral artifacts.

For optically and thermally homogeneous samples, the light source attenuates by a factor, A, at a distance x into the material [7]

$$A = \beta(\overline{\nu})\mathrm{e}^{-\beta(\overline{\nu})x} \tag{2}$$

where $\beta(\overline{\nu})$ is the wavenumber dependent optical absorption coefficient. Therefore, dampening of the source radiation by a factor of e^{-1}, e^{-2}, and $\mathrm{e}^{-2\pi}$ occurs at distances of $x = l_\beta$, $2l_\beta$, and $2\pi l_\beta$ into the sample, where the optical absorption length, l_β, is defined as

$$l_\beta = 1/\beta(\overline{\nu}). \tag{3}$$

After internal conversion of light to heat occurs within a sample, thermal waves propagate from a depth determined by the thermal diffusion length, μ_s, defined as

$$\mu_s = \left(\frac{\alpha}{\pi f}\right)^{1/2} \tag{4}$$

with the sample properties incorporated into the equation for thermal diffusivity, α, represented as

$$\alpha = \frac{\kappa}{\rho C_p} \tag{5}$$

where κ is the thermal conductivity, ρ the density, and C_p denotes the heat capacity at constant pressure. Thermal waves evolving from a depth x are proportional to e^{-ax}, where the thermal diffusion coefficient, $a = \mu_s^{-1}$; therefore, thermal wave amplitude is reduced by a factor of e^{-1}, e^{-2}, and $\mathrm{e}^{-2\pi}$ at distances of $x = \mu_s$, $2\mu_s$, and $2\pi\mu_s$ from the surface.

Eq. (4) illustrates a straightforward method of sample depth profiling using PAS, which is obtained by manipulating the Fourier frequency dependence of μ_s. The inherent weaknesses of this approach is attributed to the exponential decay of PA sensitivity with distance, thereby producing a diffuse depth resolution. Furthermore, this technique requires numerous spectra acquired at different frequencies to obtain a complete stratification model. It appears that a more efficient method to control sampling depth, which is described in this paper, can be obtained by mathematically processing the spectra obtained at 0° phase shifted (I), and 90° phase shifted (Q) with respect to the incident radiation waveform. The I spectra represent molecular information closer in proximity to the surface, whereas the Q spectra evolve primarily from the specimen bulk. Both spatially distinct spectra are easily extracted from a PA experiment by employing a digital-signal-processor (DSP) or lock-in-amplifier (LIA). With these mutually orthogonal component spectra, spatially dependent PA phase information, such as PA signal phase and phase rotation spectra, are made possible.

A physical interpretation of the PA signal phase is the time delay for thermal diffusion to occur, and the subsequent generation of an acoustic wave into the coupling gas phase. Layers deeper within a sample are resolved from shallower layers by the presence of larger phase shifts from the source radiation. The degree of phase shift can be measured using phase spectra, which is used to determine PA signal depth, especially when a nonabsorbing top layer is present in conjunction with an absorbing bottom layer at a given wavenumber [8,9]. Phase spectra are mathematically derived by applying an arctangent function on the I and Q spectra for all wavenumbers.

$$\theta = \tan^{-1}\frac{Q}{I}. \tag{6}$$

The PA signal depth can be calculated from the phase angle by first considering the equation describing one-dimensional periodic heat flow [10]. The one-dimensional heat conduction equation is represented as

$$\frac{1}{\alpha}\frac{\partial T}{\partial t} = \frac{\partial^2 T}{\partial x^2} \tag{7}$$

where T is the temperature and x the distance form the surface. The periodic sinusoidal temperature at the surface is defined as

$$T = T_0\cos(2\pi f t) \tag{8}$$

where T_0 is the temperature at $x = 0$ and t denotes time. Applying boundary conditions to the above periodic surface temperature, the following solution to Eq. (7) can be obtained:

$$T = T_0\exp(-\mu_s^{-1}x)\cos(2\pi f t - \mu_s^{-1}x). \tag{9}$$

An alternative form of Eq. (9) can be expressed as

$$T = T_0\exp(-\mu_s^{-1}x)\cos[2\pi f t - \tan^{-1}(Q/I)]. \tag{10}$$

Comparing Eqs. (9) and (10), a thermal wave from a depth x,

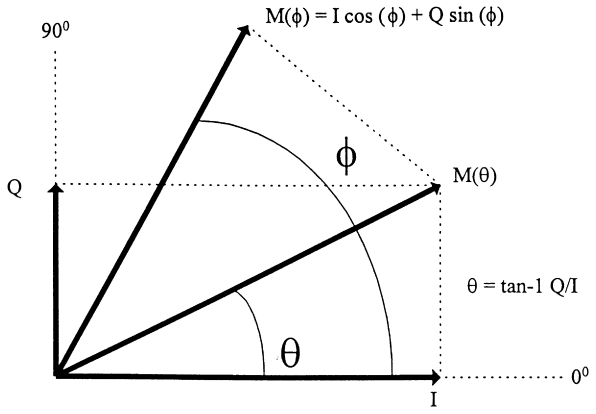

Fig. 2. Vector diagram of the *I* and *Q* signals, along with the phase rotation vectors $M(\phi)$ and $M(\theta)$, and PA phase angle, θ.

will not only possess an amplitude lower than a surface signal by a factor of $\exp(\mu_s^{-1}x)$, but will also have an associated phase lag. Using the above relationships, the depth from which the PA signal originates can be calculated using

$$x = \theta\mu_s. \tag{11}$$

Some authors have used the same phase approach to determine monolayer thickness within a sample [7–10]. However, for more accurate calculations, bands should be selected on the basis that, preferably, no contributions occur from other overlapping species. If only the band of interest absorbs at a specific wavenumber, the other layers will be optically transparent with respect to this value, allowing significant improvements in depth profiling coherence.

Similar to the PA signal phase, phase rotated spectra employ both the *I* and *Q* spectra as well. In this case, the two signals are projected onto a specific angle, ϕ, to acquire angle dependent spectra, as illustrated in Fig. 2. Further, phase spectra allow calculation of the PA signal phase delay as compared to the source, whereas phase rotation spectra determine the intensity of a band as a function of ϕ using [11]

$$M(\phi) = I\cos(\phi) + Q\sin(\phi) \tag{12}$$

or using an expression incorporating phase angle θ

$$M(\phi - \theta) = \sqrt{I^2 + Q^2}\cos(\phi - \tan^{-1}(Q/I))$$

$$= \sqrt{I^2 + Q^2}\cos(\phi - \theta). \tag{13}$$

The advantage of finding PA signal magnitude using Eq. (13), in comparison to the most frequently used magnitude calculation of

$$M = \sqrt{I^2 + Q^2} \tag{14}$$

lies in the angle dependence of phase rotated spectra. Due to the cosine function of Eq. (13), determination of the phase at a single wavenumber, followed by rotation to this angle, essentially maximizes the signal specifically for a selected wavenumber. From this phase angle dependence, a more accurate determination of signal magnitude is acquired for a given depth, as opposed to magnitude calculations employing Eq. (14).

Eqs. (6), (12), and (13) provide a mathematical description of PA phase analysis, which further enhances instrument sensitivity. From this discussion, it is evident that S^2 PAS spatial resolution can be increased using phase spectra, followed by phase rotation of the *I* and *Q* spectra.

In this study, depth profiling using phase analysis on a solid thermoplastic olefin (TPO) compound will be performed. Numerous studies illustrate the usefulness of PAS in the analysis of solid phase samples, such as TPO [12–15]. This heterogenous material consists of several components, such as polypropylene (PP), ethylene–propylene rubber (EPR), additives, and fillers to optimize physical and chemical properties. A low percentage of EPR is added to the compound to increase the surface energy of TPO, thereby acting as an adhesion promoter, while the relatively higher percentage of PP reduces composite density, and increases overall durability. TPO additives include thermal and process stabilizers, ultraviolet absorbers, pigments, and fillers. Talc is used as a filler in TPO, which not only improves the overall material properties, but is also responsible for increasing mechanical properties, enhancing surface quality, lowering mold shrinkage, and improving compound processing as well.

Due to a limited amount of a priori knowledge of the absorbing layer depth, systems such as TPO present a greater challenge in extending the PA phase theory to an experiment. The presence of nonoverlapping bands allows acquisition of a unique phase angle for every absorbing layer in a compound, such as TPO. In the case of homogenous samples, absorption occurs at all depths for a single vibrational mode, resulting in a shallow penetration depth versus a sample with nonabsorbing top layers.

The intent of this paper is twofold: (1) to present a method to increase spatial resolution by further developing PA analysis using phase and phase rotation spectra, and (2) to qualitatively and quantitatively apply phase information to determine the component distribution within a TPO sample. This objective will be achieved by using S^2 PAS instead of CS PAS, due to its ability to extract phase information; and reduce multiple signals from spatially heterogeneous layers.

2. Experimental

Single-beam spectra were acquired using a Nicolet Magna-IR System 850 optical bench, purged with CO_2-free dry air, and a He-purged MTEC 100 photoacoustic cell. He coupling gas (99.999%) was chosen for the experiment due to its superior thermal coupling properties, allowing enhancement of the photothermal sensitivity. Phase modulation of the IR light was accomplished at an amplitude of

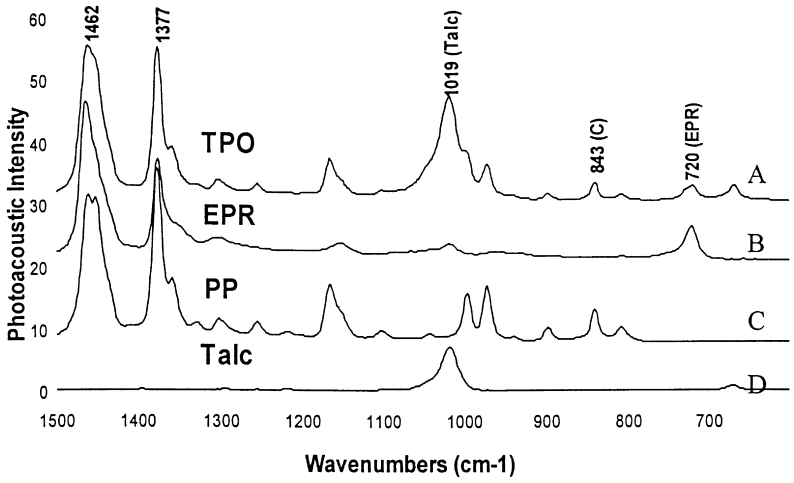

Fig. 3. PA FT-IR spectra of TPO and individual components: (A) TPO; (B) EPR; (C) PP; and (D) talc.

two laser-fringe (1.266 μm retardation, or two He–Ne laser wavelengths, $\pm 2\lambda_{He-Ne}$), with the interferometer step scanning at 25 Hz (632.8 nm retardation shift/step). Simultaneous acquisition of the *I* and *Q* signals, and subsequent conversion using an analog-to-digital converter (ADC) allowed the phase angle spectra and phase rotation spectra to be acquired using Nicolet OMNIC 3.1a FT-IR software for modulation frequencies of 1000, 800, 600, 400, and 300 Hz at 8 cm^{-1} resolution. The reference angle for each modulation frequency was determined using a 60% carbon-black-filled elastomer (MTEC). Injection-molded 3.8 mm thick TPO plaques with oxidative stabilizers, 5.0 mm thick EPR plaques, and 2.5 mm thick polypropylene were obtained from the Ford Motor Company. Talc[magnesium silicate, $Mg_3(OH)_2Si_4O_{10}$], used for a reference spectrum, was acquired from the Mallinckrodt Company.

3. Results and discussion

Previous spectroscopic depth profiling studies showed evidence of substantial changes in film properties as a result of individual polymeric components distributing throughout a surface [16–22]. One issue of pertinent interest related to TPO surface stratification concerns poor adhesion, resulting from the low surface energy (~30 mN m^{-1}) of the substrate [23]. As several preceding studies demonstrate, this intrinsic property is mainly ascribed to surface stratification processes in TPO, where constituents migrate into separate discrete layers as a result of various surface energies, physical properties, and processing methods [23,24]. For example, injection-molding results in TPO components such as talc, PP, and EPR separating into discrete layers due to applied shear forces and thermal gradients during processing. The processing conditions not only separate components, but also produce morphological changes near the surface. This effect may alter cohesion by creating weak boundary layers between each layer, and may diminish adhesion between a coating and TPO [24]. Even though several techniques display viable surface characterization abilities, the destructive nature of many experimental methods make these experiments inappropriate for certain studies [16–22]. For example, microtoming of TPO may cause formation of a crystalline layer at the surface, resulting from applied shear forces promoting polymer chain alignment. Besides offering surface analysis capabilities, the PA technique used in this study also performs depth profiling experiments in a nondestructive manner.

Table 1
Thermoplastic olefin (TPO) component band assignments for the spectral range of 1100–700 cm^{-1}

Component	Wavenumber (cm^{-1})	Assignment[a]
Talc	1019	ν(Si–O)
PP	999	δ(–CH) + ρ(C–C) + ω(C–CH_3)
PP	973	ρ(CH_3) + ω(C–C)
PP	843	ν(C–CH_3) + ρ(CH_2)
EPR	720	ρ(CH_2) in-plane

[a] ν = stretching, ρ = rocking, ω = wagging, δ = deformation.

As shown in one of our previous studies, stratification of TPO was detected using the wavenumber dependence of CS PAS [25]. These studies concluded that the majority of the uppermost surface layers consist of talc and crystalline PP, whereas EPR and amorphous PP components extend further into the bulk; confirming previous TPO stratification findings using other techniques [24]. In order to further elucidate TPO component distribution, this study focuses on developing a S^2 PAS method, utilizing the features already mentioned.

Fig. 3 illustrates a spectrum of TPO (trace A), along with spectra of its individual components: EPR (trace B), PP (trace C), and talc (trace D). The spectral range from 1100 to 700 cm^{-1} exhibits several vibrational features unique to each of the three components of interest. The corresponding band assignments for each of these features, including the responsible absorbing species, is presented in Table 1. From

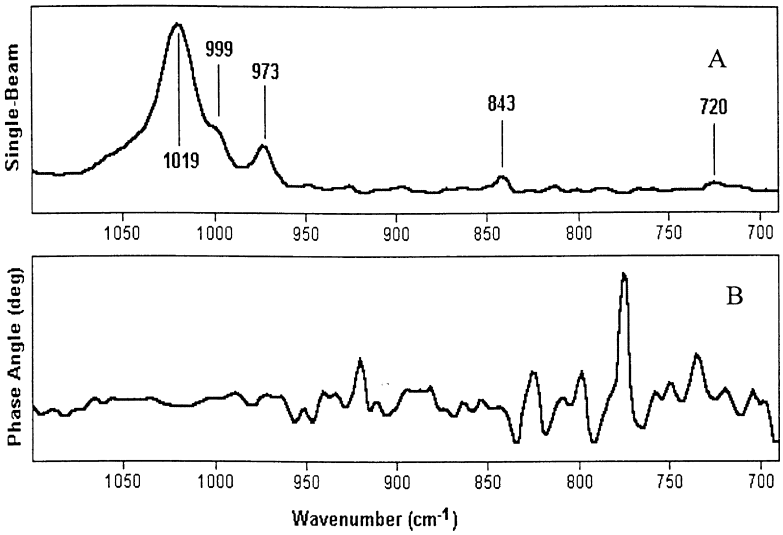

Fig. 4. Single-beam (A) and phase angle spectra (B) of TPO at 1000 Hz modulation frequency in the range 1100–690 cm^{-1}.

this table, evidence of the band attributed to the Si–O stretching vibrations of talc, is detected at 1019 cm^{-1}. PP contributions to the TPO spectrum are located at 999 cm^{-1} (CH_3 rocking, CH_2 wagging, and CH bending modes), 973 cm^{-1} (CH_3 rocking mode, and C–C chain stretching), and 843 cm^{-1} (C–CH_3 stretch and CH_2 rock) [26]. The band centered at 720 cm^{-1}, due to CH_2 in-plane rocking vibrations, results from the presence of EPR elastomer. Of particular interest to a TPO sample spectra are the intensity changes of two PP bands, 999 and 843 cm^{-1}, attributed to the content of crystalline domains in PP [27]. As shown by Ryntz, improved adhesion to TPO has been ascribed to the rearrangement of PP crystallites at the uppermost surface, promoting mechanical interlocking between the coating and the substrate [24].

In order to enhance the spatial resolution of the surface depth-profiling experiment, a wide range of modulation frequencies were examined. These experimental frequencies representing various depths indicate significant differences in both PA single-beam and phase angle spectra. Figs. 4 and 5 show the two extreme frequency limits of both single-beam (traces A) and phase angle spectra (traces B) acquired at 1000 and 300 Hz. Significant differences among the series of single-beam PA intensity spectra is observed as frequency decreases due to greater thermal diffusion lengths. Fig. 6, along with Table 2, show the measured experimental phase angles, θ, of each TPO component, along with their respective wavenumbers. Since each modulation frequency represents a different depth from where PA signal derivation occurs, the associated phase lag (or time delay) will also vary with frequency. This indicates that, if a PA signal originates close to the surface–gas interface, the

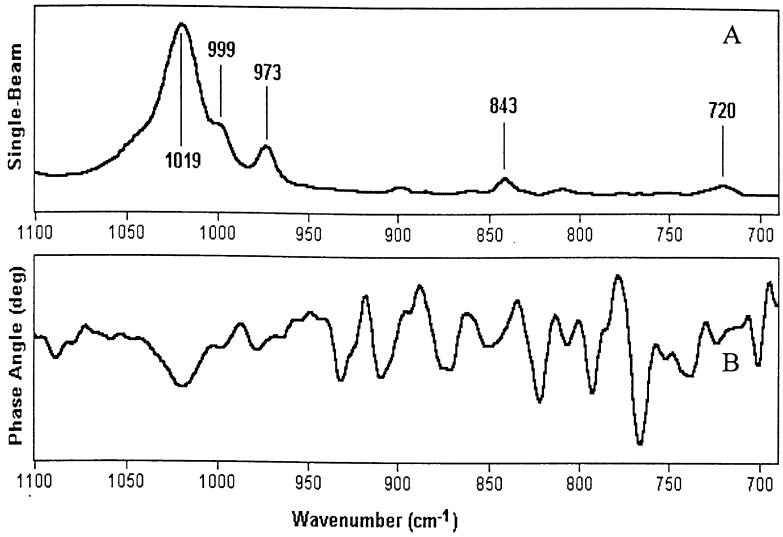

Fig. 5. Single-beam (A) and phase angle spectra (B) of TPO at 300 Hz modulation frequency in the range 1100–690 cm^{-1}.

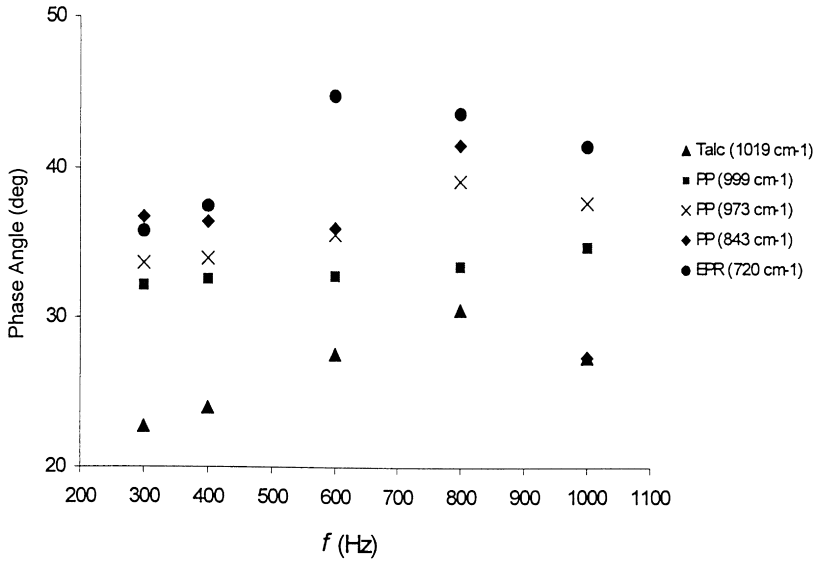

Fig. 6. Plot of PA phase angle, θ (degrees), versus modulation frequency, f (Hz), for talc, PP, and EPR components of TPO.

phase angle calculated from the I and Q spectra should be relatively low in magnitude. Several PA studies used phase information from the I and Q components as a measurement for spectral depth profiling for thin multilayer films [8,9,11]. In each case, analysis was simplified by the fact that the thickness of each homogenous layer was known. Since the system used in this study stratifies into separate layers near the surface, the same principles can be applied.

With these considerations in mind, we will first examine a set of data taken at a single modulation frequency. Visual inspection of the phase relationship of the absorbing layers at $f = 300$ Hz, presented in Fig. 6 and Table 2, shows the ascending phase order for a specific wavenumber as follows: 1019 cm^{-1} (Si–O stretching region), 999 cm^{-1} (CH_3 rocking, CH_2 wagging and CH bending modes), 973 cm^{-1} (CH_3 rocking mode, and C–C chain stretching), 720 cm^{-1} (CH_2 in-plane rocking), and 843 cm^{-1} band (C–CH_3 stretch and CH_2 rock). Assigning these wavenumbers to their corresponding components, the layer ordering of the species from sample surface to bulk consists of talc, PP, EPR, and PP. Comparing these values to data acquired at a higher modulation frequency (1000 Hz), the phase values for each band can be arranged in ascending order as: 1019 cm^{-1} (Si–O stretching region)/843 cm^{-1} band (C–CH_3 stretch and CH_2 rock), 999 cm^{-1} (CH_3 rocking, CH_2 wagging and CH bending modes), 973 cm^{-1} (CH_3 rocking mode, and C–C chain stretching), and 720 cm^{-1} (CH_2 in-plane rocking), or with respect to their components, talc/PP, PP, and EPR. A noteworthy feature of these data acquired closest to the surface (1000 Hz) is the presence of the PP crystalline bands at 843 and 999 cm^{-1}, consistent with previous TPO studies [24]. Further, the layering of the chemical species between the two frequencies appears consistent; however, a comparison of the phase values of the two frequencies shows that the 1000 Hz frequency has significantly larger phase angles, in contrast to values obtained at 300 Hz. Since the signal collected at 300 Hz travels through a greater amount of sample (as opposed to 1000 Hz), intuitively, the expected phase angle for 300 Hz should be greater than the phase value produced at 1000 Hz. Therefore, when comparing phase angles taken at different modulation frequencies, a phase shift correction taking into account the instrumental phase, as well as signal depth for a given frequency, must be applied to the original phase angle.

Studies performed by Bertrand [28], in addition to those performed by Roark and Palmer [29], suggest obtaining all data for a single modulation frequency at a reference angle determined by maximizing the interferogram peak height for a highly absorbing species, such as carbon black. Indeed, the proposed technique maximizes the signal for a given frequency, however, this method does not necessarily assure that each signal originates from the same depth for a sample

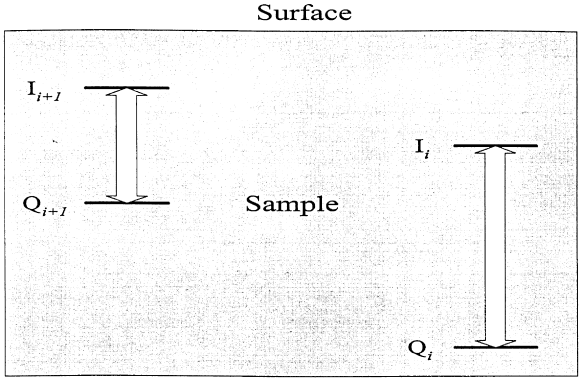

Fig. 7. PA diagram showing the relative distribution of the I and Q spectra, where the $i + 1$ frequency is the next sequential highest frequency from the ith frequency.

at different frequencies. In order to relate data from different modulation frequencies, dependence of the thermal wave origin on modulation frequency and detection angle should be considered. Obtaining spectra at a specific collection angle, does not necessarily assure that the *I* and *Q* channels begin to collect data from the same depth within the sample. The notion of the *I* and *Q* spectra originating from different depths for different modulation frequencies can be proven experimentally by comparing the band intensities of these spectra at different frequencies, such as those shown in Table 3. *I* and *Q* single-beam spectra taken at a low modulation frequency, *i*, will have a greater magnitude than those acquired with a higher frequency, $i + 1$. Therefore, both signals must originate from deeper depths and possess greater path lengths for lower modulation frequencies, as shown Fig. 7. Further support of this approach can be found by analyzing the data in Fig. 8 and Table 4. After taking into account collection angle differences for each frequency, φ, and incorporating these values to the phase, θ, the experimental phase angles, θ', are now consistent with theory. This was performed by calculating the difference between the reference angle taken at 1000 Hz and the angles acquired at other frequencies, and adding these phase shifts into the values measured from the experimental phase spectra, θ, to acquire the corrected phase, θ'.

Using Eq. (11), and selecting bands with marginal contributions from other species, the depth can be determined for each component layer. Therefore, we will

Table 2
Phase angle data, θ (degrees), for each TPO component taken at modulation frequencies of 300–1000 Hz

Component	Wavenumber (cm^{-1})	θ				
		300 Hz	400 Hz	600 Hz	800 Hz	1000 Hz
Talc	1019	22.7	24.0	27.6	30.6	27.4
PP	999	32.2	32.6	32.8	33.4	34.7
PP	973	33.6	33.9	35.5	39.1	37.6
PP	843	36.7	36.4	36.0	41.6	27.4
EPR	720	35.7	37.4	41.4	43.7	42.0

Table 3
Band heights of *I* and *Q* single beam spectra for 300 and 800 Hz modulation frequency for various wavenumbers

Component	Wavenumber (cm^{-1})	*I* (300 Hz)	*Q* (300 Hz)	*I* (800 Hz)	*Q* (800 Hz)
Talc	1019	0.917	0.384	0.290	0.171
PP	843	0.0811	0.0605	0.0284	0.0252
EPR	720	0.0500	0.0359	0.0186	0.0178

Table 4
Corrected phase angle, θ' (degrees), for each TPO component taken at modulation frequencies of 300–1000 Hz

Component	Wavenumber (cm^{-1})	θ'				
		300 Hz	400 Hz	600 Hz	800 Hz	1000 Hz
Talc	1019	46.7	41.0	37.6	35.6	27.4
PP	999	56.2	49.6	42.8	38.4	34.7
PP	973	57.6	50.9	45.5	44.1	37.6
PP	843	60.7	53.4	46.0	46.6	27.4
EPR	720	59.7	54.4	51.4	48.7	42.0

Table 5
Calculated depths, *x* (μm), of 1019 cm^{-1} (talc), 843 cm^{-1} (PP), and 720 cm^{-1} (EPR) components for modulation frequencies of 1000, 800, 600, 400, and 300 Hz

Component	Wavenumber (cm^{-1})	*x*				
		1000 Hz	800 Hz	600 Hz	400 Hz	300 Hz
Talc	1019	2.67	3.91	4.79	6.37	8.40
PP	843	2.67	5.12	5.86	8.29	10.9
EPR	720	4.11	5.35	6.55	8.45	10.7

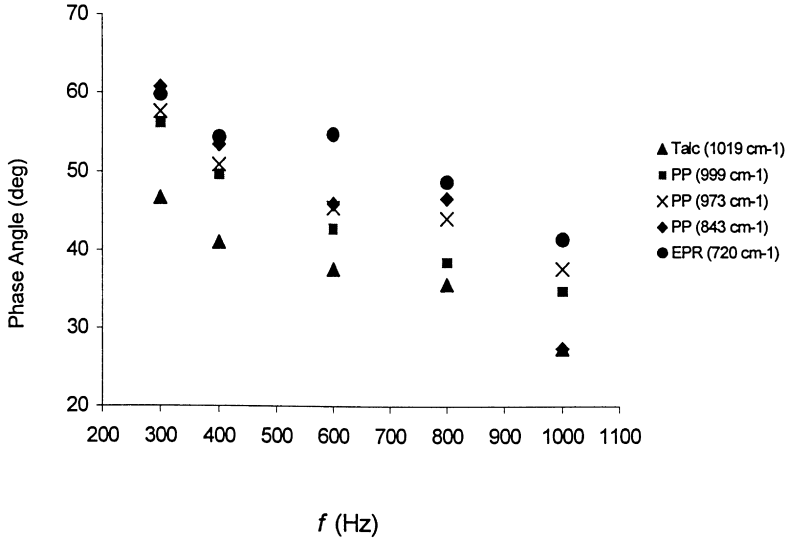

Fig. 8. Plot of the corrected PA phase angle, θ' (degrees), versus modulation frequency, f (Hz), for talc, PP, and EPR components of TPO.

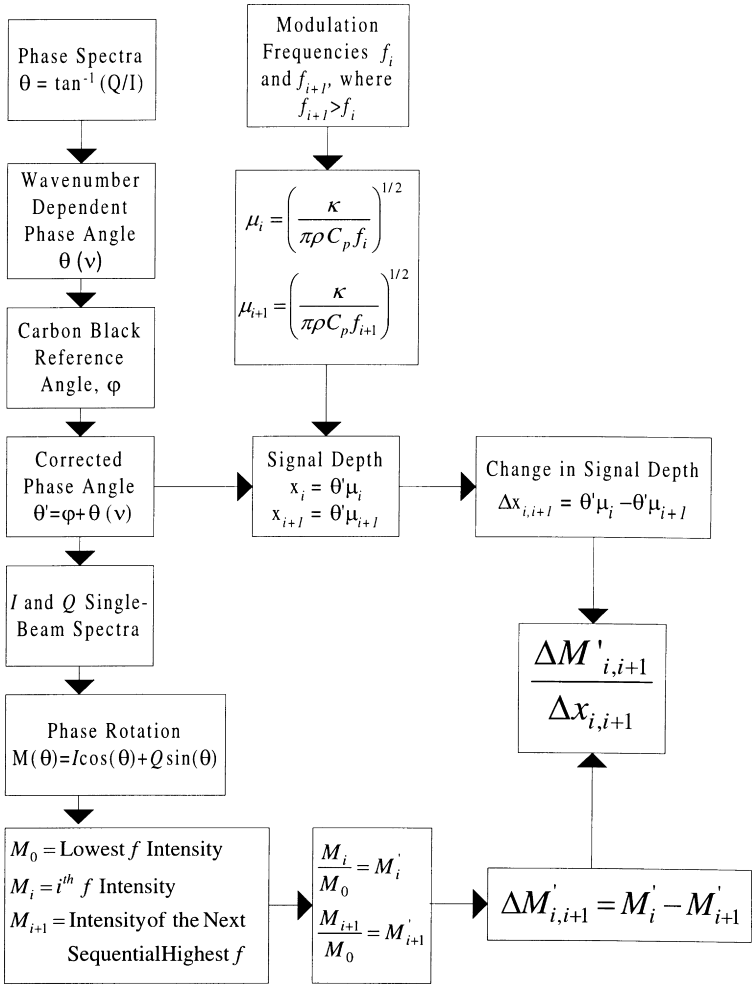

Fig. 9. TPO stratification phase analysis algorithm.

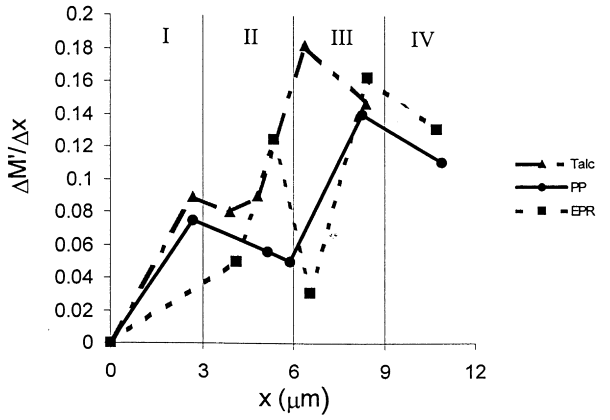

Fig. 10. Plot of the rotation magnitude derivative, $\Delta M'/\Delta x$, with respect to distance, x (μm), into the TPO sample.

apply the above approach to the bands at 1019, 843, and 720 cm^{-1} as probes for talc, PP, and EPR, respectively. The values used to calculate α and, ultimately, μ_s were: $\kappa = 0.148$ W m^{-1} K^{-1}, $\rho = 0.98$ g ml^{-1}, and $C_p = 1.58$ J g^{-1} K^{-1}. From these values, the PA signal depth for each species shown in Table 5 was calculated, followed by determination of the change in depth, $\Delta x_{i,i+1}$, with each incremental change in frequency, where $f_i < f_{i+1}$. Once the phase angle and change in depth for each species is established, the I and Q spectra are phase rotated with respect to the experimental phase, θ, using Eq. (12). This is performed for all experimental frequencies, proceeded by measurement of the band height, $M(\theta)$, for a specific component at its respective phase angle, since the band height is at a maximum at this angle, as evident from Eq. (13). The calculation proceeds by determining the ratio of the heights at higher frequencies, M_i and M_{i+1}, with respect to the lowest frequency, M_0. The analysis is completed by determining the derivative of the rotation magnitude with respect to x, $\Delta M'_{i,i+1}\Delta x_{i,i+1}$, allowing determination of the relative change in concentration with depth. An algorithm used for the entire process is illustrated in Fig. 9, and a plot showing the above calculation applied to the TPO data is presented in Fig. 10.

Performing the above process and by inspection of Fig. 10, a stratification model for the TPO system can be proposed. For convenience, the derivative plot in Fig. 10 was separated into four distinct layers. Layer I, extends from 0 to 3 μm from the surface, and displays talc as the component with the highest concentration change, reaching a local maximum at 2.7 μm. A more diffuse concentration is exhibited with PP in this layer, as shown by the relatively broad peak extending into layer II (3–6 μm). At the onset of this layer, the talc concentration change drops to a minimum; however, PP shows the overall local minimum for this layer, with a large decrease at 5.86 μm. An abrupt increase in EPR concentration, which serves as the local maximum for this layer, is observed at 5.35 μm from the surface. Additional substantiation for this behavior is shown from results of other studies of multiphase PP/EPR blends displaying evidence of EPR existing as discrete particle phases embedded within a PP matrix [30–32]. Extending further from the surface into layer III (6–9 μm), talc and PP concentrations begin a sharp incline, whereas EPR significantly declines. Within this same layer, changes in talc concentration reach a maximum, and eventually show a decrease in the derivative plot with increasing distance from the surface, until it reaches the furthest detected depth at 8.4 μm. Layer III also shows the greatest change in the plot for both talc and PP for distances of 0–12 μm. The concentrations of both of these components decrease as the depth increases from 9 to 12 μm (layer IV). Layer IV also shows further evidence of EPR phase segregation, with a large increase at 8.45 μm.

4. Conclusions

In this study we have demonstrated a S^2 PAS phase analysis method to determine a stratification model of a TPO compound using both phase angle and phase rotation calculations. The model is consistent with previous studies, however, utilizing this method provides a substantial increase in spatial resolution, thereby improving the accuracy of the proposed model. An adequate description of our model separates a TPO sample into four separate layers extending from 0 to 12 μm from the surface. At 0–3 μm, from the surface (layer I) a high concentration change of talc and PP is evident. Within layer II (3–6 μm), both talc and PP concentrations decrease, with EPR concentration increasing with a local maximum for this region. This region between 3 and 6 μm also shows the component segregation behavior with evidence of particles composed of an EPR core embedded within a PP matrix. However, at the onset of layer III, an increase in both talc and PP concentration is observed, followed by a decrease as the distance from the surface approaches 9 μm. Within this same layer, the change in EPR concentration increases to its highest value for all distances, 0–12 μm. Both the PP and EPR components extend into the bulk of layer IV (9–12 μm), with no talc detected within this area.

In addition to proving the technique useful for the analysis of compound surfaces, the developed PA model can readily be applied to other systems displaying stratification phenomena, allowing unlimited depth profiling possibilities.

Acknowledgements

The authors would like to thank the National Science Foundation Industry/University Cooperative Research Center in Coatings at North Dakota State University and Eastern Michigan University for financial support of these studies.

References

[1] Rosencwaig A. Photoacoustics and photoacoustic spectroscopy. New York: Wiley, 1980.
[2] McClelland JF. Anal Chem 1983;55:89A.
[3] Smith MJ, Manning CJ, Palmer RA, Chao JL. Appl Spectrosc 1988;42:542.
[4] Griffiths PR, DeHaseth JA. Fourier transform infrared spectrometry, Chemical Analysis Series 83. New York: Wiley, 1980.
[5] Manning CJ, Griffiths PR. Appl Spectrosc 1997;51:1092.
[6] Dittmar RM, Palmer RA, Carter RO. Appl Spectrosc Rev 1994;29:171.
[7] Palmer RA, Dittmar RM. Thin Solid Films 1993;223:31.
[8] Jiang EY, Plamer RA. J Appl Phys 1995;78:460.
[9] Jiang EY, Palmer RA, Barr NE, Morosoff N. Appl Spectrosc 1997;51:1238.
[10] Adams MJ, Kirkbright GF. Analyst 1977;102:281.
[11] Jones RW, McClelland JF. Appl Spectrsoc 1996;50:1258.
[12] Mandelis A, Teng YC, Royce BS. J Appl Phys 1979;50:7138.
[13] Urban MW, Koenig JL. Appl Spectrosc 1986;40:994.
[14] Ludwig BW, Urban MW. Polymer 1993;34:3376.
[15] Ludwig BW, Urban MW. Polymer 1994;35:5130.
[16] Ludwig BW, Urban MW. J Coat Technol 1994;66:59.
[17] Niu BJ, Urban MW. J Appl Polym Sci 1996;62:1903.
[18] Niu BJ, Urban MW. J Appl Polym Sci 1995;56:377.
[19] Niu BJ, Urban MW. J Appl Polym Sci 1996;60:389.
[20] Evanson KW, Urban MW. J Appl Polym Sci 1991;42:2297.
[21] Evanson KW, Urban MW. J Appl Polym Sci 1991;42:2309.
[22] Kaminski AM, Urban MW. J Coat Technol 1997;69:113.
[23] Prater TJ, Kaberline SL, Holubka JW, Ryntz RA. J Coat Tech 1996;68:83.
[24] Ryntz RA. Prog Org Coat 1996;27:241.
[25] Pennington BD, Urban MW, Ryntz RA. Polymer 1999;44:4795.
[26] Tadokoro H, Kobyayashi M, Ukita M. J Chem Phys 1965;42:1432.
[27] Miyazawa T, Fukushima K, Ideguchi Y. J Polym Sci Part B 1963;1:385.
[28] Bertrand L. Appl Spectrosc 1988;42:134.
[29] Roark JC, Palmer RA. Chem Phys Lett 1978;60:112.
[30] Mirabella FM. Polymer 1993;34:1729.
[31] Mirabella FM. J Polym Sci, Part B: Polym Phys 1994;32:1205.
[32] Mirabella FM. Polymer 1996;37:931.